THS

LIBRARIES MICHIGAN STATE UNIVERSITY EAST LANSING, MICH 48824-1048

This is to certify that the thesis entitled

ULTRAFAST DYNAMICS OF POLYATOMIC MOLECULES UNDER INTENSE LASER RADIATION

presented by

Vahan Artsruni Senekerimyan

has been accepted towards fulfillment of the requirements for the

M.S.	degree in	Chemistry	
	Con	Luz	
	Major Pro	ofessor's Signature	
	Ju	ne 11,04	
		Date	

MSU is an Affirmative Action/Equal Opportunity Institution

PLACE IN RETURN BOX to remove this checkout from your record. TO AVOID FINES return on or before date due. MAY BE RECALLED with earlier due date if requested.

DATE DUE	DATE DUE	DATE DUE

6/01 c:/CIRC/DateDue.p65-p.15

ULTRAFAST DYNAMICS OF POLYATOMIC MOLECULES UNDER INTENSE LASER RADIATION

BY

Vahan Artsruni Senekerimyan

A THESIS

Submitted to
Michigan State University
in partial fulfillment of the requirements
for the degree of

MASTER OF SCIENCE

Department of Chemistry

2004

ABSTRACT

ULTRAFAST DYNAMICS OF POLYATOMIC MOLECULES UNDER INTENSE LASER RADIATION

BY

Vahan Artsruni Senekerimyan

The goal of the research was to develop methods to study and control the behavior of molecules on an ultrashort time-scale. First, the behavior of molecules under high intensity femtosecond laser irradiation is discussed. In this part, we discuss the electric field produced by the lasers, and how this field interacts with molecules causing multiphoton or field ionization and Coulomb explosion. Results obtained with the help of femtosecond CPM dye laser and molecular beam apparatus coupled with a time-of-flight mass spectrometer are shown for triatomics such as CS₂ and NO₂. Analysis of angular distributions of molecular and fragment ions of these molecules is presented and structural information of Coulomb exploding molecular ions of CS₂ is retrieved. Second, preliminary experimental and theoretical results for ozone are presented. It is shown that ozone does not behave like NO₂ or CS₂ under the same experimental conditions. Possible explanations of this result are discussed.

ACKNOWLEDGMENTS

I would like to thank my adviser Professor Marcos Dantus and all Dantus research group members and express thanks to my Guidance Committee members -

Professors John McCracken, Katharine Hunt, and Jack Watson for their help and comments. I am also grateful to Professor Kaoru Yamanouchi from University of Tokyo for giving me permission to use a figure from his article in Science (Science, 295, 1659-1660, 2002) in my thesis.

TABLE OF CONTENTS

LIST OF TABLES	vi
LIST OF FIGURES	vii
INTRODUCTION	1
EXPERIMENTAL	7
EXPERIMENTAL RESULTS	9
Experimental results of Coulomb explosion in CS ₂ and NO ₂	
DISCUSSION	13
CONCLUSIONS	18
APPENDICES	20
Appendix A	21
Figure 1	22
Appendix B	
Figure 2	
Appendix C	
Figure 3	
Appendix D	
Figure 4	
Appendix E	
Figure 5	
Appendix F	
Figure 6	32
Appendix G	
Figure 7	
Appendix H	
Figure 8	
Appendix I	
Figure 9.	
Appendix J	

Figure 10	
Figure 11	
BIBLIOGRAPHY	43

LIST OF TABLES

Table 1. First and second vertical ionization potentials (VIP) of ozone and	
O_3^+ and O_3^{2+} obtained in the CCSD(T) calculations	12
Table 2. Comparison of experimental values of first and second ionization	potentials of
O ₃ , CS ₂ , CO ₂ , SO ₂ , and NO ₂	16

LIST OF FIGURES

Figure 1. Laser field induced processes in various intensity regimes (from K Yamanouchi: Science 295 (2002) 1659-60)
Figure 2. Schematic of 3-step multiphoton ionization in two cases: resonant (on the left) and non-resonant (on the right). Typical laser electric field intensities required for these two processes are $1-10^4$ W/cm ² and $>10^{12}$ W/cm ² for resonant and non-resonant processes respectively. Non-resonant absorption of the photon proceeds through the virtual state with lifetimes on the order of 1 fs
Figure 3. Schematic representation of field (tunneling) ionization for an atomic system. Keldysh adiabaticity model is reasonable for field ionization when $\gamma = T_{tunnel}/T_{laser} << 1$. In the opposite limit multiphoton ionization mechanism is appropriate
Figure 4. a) Schematic for the experimental setup. b) Schematic representation of the Coulomb explosion process leading to the splitting in the mass spectrum (from Comstock M, Senekerimyan V, Dantus M: J Phys Chem A 107 (40): 8271-8281 2003)28
Figure 5. Glass container with the stored ozone on silica gel in the isopropyl/dry ice slurry bath at around - 85° C (from V Senekerimyan, M McGuire, M Comstock, M Dantus: Quantum Control of Light and Matter, Gordon Research Conference, Mount Holyokee, MA 2003)
Figure 6. a) Mass spectrum of CS ₂ , where the zoomed part shows the splitting of the peaks. b) The isotropic angular distribution of the CS ₂ ⁺ parent ion (from Comstock M, Senekerimyan V, Dantus M: J Phys Chem A 107 (40): 8271-8281 2003)32
Figure 7. Angle dependent detection of singly and doubly charged fragment ions following Coulomb explosion. pronounced. S ²⁺ shows a maximum ion yield at 0° and 180°, while C ²⁺ shows a maximum at 90° and 270° (from Comstock M, Senekerimyan V, Dantus M: J Phys Chem A 107 (40): 8271-8281 2003)
Figure 8. Mass spectrum of NO ₂ taken at laser peak power 4.6×10 ¹⁴ W/cm ² . Notice the splitting in the peaks of N ⁺ and O ⁺ (from V Senekerimyan, M McGuire, MComstock, M Dantus: Quantum Control of Light and Matter, Gordon Research Conference, Mount Holyokee, MA 2003)
Figure 9. a) Mass spectrum of O_3 (top) and air (bottom) taken under the same experimental conditions as that of NO_2 . The dashed arrow points where O_3^{2+} should

appear. (b) Polar plot of angular distribution for O ₂ ⁺ (solid line) and O ⁺ (dashe	
twice reduced in scale) (from V Senekerimyan, M McGuire, M Comstock, M	
Quantum Control of Light and Matter,. Gordon Research Conference, Mount	Holyokee,
MA 2003)	38
Figure 10. Conceptual drawings of the Coulomb Explosion of CS ₂ when the east parallel or perpendicular to the time-of-flight axis for the a) linear molecule	
bent molecules	40
Figure 11. A typical potential energy curve for the diatomic dication	42

1. Introduction

Electric forces underlie almost all of chemistry and molecular physics. Precise manipulation of external electric fields, therefore, may be a natural choice to explore the study and control of atomic and molecular dynamics. Ultrashort lasers allow probing of molecular processes in real time on the femtosecond time scale (1). Another unique feature of these lasers is the ability to get extremely high peak powers. The advent of modern amplification methods has greatly increased the output energies of femtosecond pulses. Today even in small university labs, laser fields with peak powers as high as 10¹⁸ W/cm² can be routinely generated; this intensity is comparable in magnitude to the intensity generated by the atomic nucleus. For instance, the electric field strength of a 10¹⁸ W/cm² pulse is approximately 5*10⁹ V/cm, which is the same as the hydrogen intratomic field.

Such fields will help in studying atomic and molecular processes, and will cause a number of physical phenomena in atoms and molecules such as multiphoton or field ionization, structural deformations, and Coulomb explosion (CE). The behavior of molecules in such fields has been studied intensively in the last decade to clarify complex dynamics caused by the interplay among electrons, nuclei, and a photon field.

When electric field intensities approach 10¹⁰ W/cm², the alignment of molecules along the laser field direction takes place (Fig. 1). At these intensities, the probability of

ionization is low, thus, we can investigate the alignment mechanism of neutral species subjected to the laser field.

The next electric field intensity regime, where one may observe structural deformations of molecules, multiple ionization, and Coulomb explosion, is reached when the field intensity is increased to between $10^{13} - 10^{16}$ W/cm². In this power region, which is called Coulombic regime (Fig.1), the removal of two or more electrons via the muliphoton or field ionization leads to CE because of the strong Coulombic repulsion in the resulting positively charged molecular ion island (2). Thus, it is the multiple ionization that leads to CE. A simple schematic for resonant and non-resonant multiphoton ionization is given in Figure 2. In case of non-resonant ionization, the absorption of photons proceeds through the virtual states having lifetimes on the order of 1 fs. Therefore, non-resonant multiphoton absorption requires much higher laser field power compared to the case of resonant absorption. Resonant absorption of photons enormously facilitates the transitions; therefore, the multiphoton absorption probability is dependent on the laser wavelength resonant or non-resonant with the molecular transitions. A simple schematic for field ionization (also called tunneling ionization) for an atomic system is shown on Figure 3. As an approximation, we may treat the effective electric field due to the laser as a static field. That is, we will assume we can ignore the fact that the field actually oscillates sinusoidally in time. If we combine the Coulomb potential of the nucleus, q/r, with the static field potential, eEr, the electrons then move in a distorted potential similar to that shown in Figure 3. The central features of this potential are (1) the electrons are only quasi-bound in one side of the potential since they can tunnel through the barrier to freedom and (2) the higher the intensity, the more the ground state energy level (potential barrier) is pushed upward. Clearly at some intensity the ground level may reach the top of the barrier. This occurs at about 10¹⁴ W/cm² for the ground state of the hydrogen atom. It turns out that this is also true for many electron systems; they too will not survive as neutral species at intensity of about 10¹⁴ W/cm². This field ionization picture depends on the validity of treating the laser field as a static electric field. This Keldysh adiabaticity model is reasonable if there is enough time for the electron to escape before the direction of field changes sign. Often the Keldysh parameter (3) is used as a measure of when the static field approach is valid. When the Keldysh parameter, given by

$$\gamma = \omega_{laser}/\omega_{tunnel} = T_{tunnel}/T_{laser} = (U_{IP}/1.87*10^{-13}*I*\lambda^{2})^{1/2},$$
 (1)

is <<1, the field approach is a reasonable assumption. In Eq. (1) U_{IP} is the ionization potential of the atom, I the intensity in W/cm² and λ the wavelength in microns. In the opposite limit it is appropriate to view ionization as a multiphoton process and employ perturbation theory to determine the ionization rate. For molecular systems, by convention when $\gamma < 0.5$ the system is in the tunnel ionization regime, otherwise it is in multiphoton ionization regime.

When the laser field intensity is increased to 10^{14} - 10^{15} W/cm², strong mixing of electronic states also occurs. This implies that the potential energy surface (PES) of the molecule, whose shape is determined by the electronic configuration, becomes deformed (4). Since the angular distributions of fragment ions following CE will be sensitively dependent upon the geometry of exploding molecular ions, the molecular and ionic

deformations resulting from the formation of these light-dressed states may be investigated by studying the angular distributions of the fragment ions ejected upon CE and analyzing them either by mass-resolved momentum imaging (MRMI) or coincidence momentum imaging (2,5).

In fact, the dynamics in Coulombic regime is rather complex. This kind of research helps us understand the fundamentals and nature of high intensity laser and matter interactions and serves as a good tool in investigating the behavior of molecules subject to laser fields. The ability to apply strong electric forces with high precision and little energy has led to various applications in science and technology. For example, intense femtosecond lasers have found their way as novel ionization sources in mass spectrometry. There is also a great commercial interest to femtosecond laser machining of materials due to the high precision and reduced local heat deposition of this process. Studies of atmospherically relevant molecules such as O₃, CS₂, CO₂, NO₂, O₂, H₂O, etc in high - intensity laser fields is also important since it will allow us to understand how the molecules and the laser field are modified during the propagation of the pulses in the atmosphere.

As will be shown in this work, not all the molecules subject to high - intensity fields in the Coulombic regime behave similarly, which may be caused by the multiple ionization dependence on laser wavelength. A number of dissociation channels may be accessed, each having a partial cross section depending upon the focused laser peak intensity, laser wavelength, and pulse duration. For instance, for CS_2 we observe CS_2^{2+} , CS_2^{3+} , CS_2^{4+} , etc in the mass spectrum, which Coulomb explode producing different fragment ions via various channels. For example, $CS_2^{3+} \rightarrow CS^+ + S^+ + C^+$, $CS_2^{3+} \rightarrow S^{2+} + CS_2^{3+} \rightarrow S_2^{3+} \rightarrow S_2^{3+$

 CS^+ , or $CS_2^{3+} \to C^+ + 2S^+$, $CS_2^{4+} \to S_2^{2+} + C^{2+}$, etc. The identification of dissociation channels is also a quite complicated aspect since some of the exploding molecular ions may not be present in the TOF mass spectrum. This happens when the lifetime of the multiply charged ion is shorter than the time of flight in the TOF spectrometer.

Experimentally, one can vary the wavelength, risetime, focused intensity and state of polarization of the laser and measure the kinetic energy and angular distributions of the photoions or photoelectrons. One usually uses time-of-flight (TOF) spectroscopy for such measurements.

At laser field intensities about 10¹⁷ W/cm² and higher, we can observe X-Ray emission and nuclear fusion (See Fig.1). At 10²⁰ W/cm², we approach the electric field strengths comparable to intranuclear forces, which can cause nuclear fusion. This is another hot scientific topic nowadays, and scientists are trying to take advantage of ultrafast lasers to generate highly energetic proton and electron beams, electron-positron pairs, and use them for plasma and astrophysical research.

Here I present experimental studies of triatomics such as CS₂, NO₂, and O₃ under high intensity laser irradiation in the Coulombic regime. TOF mass spectra of these molecules following Coulomb explosion are collected along with the angular distributions of molecular and fragment ions of CS₂ and O₃. Data analyses are made to retrieve structural information about exploding molecular ions of CS₂. Preliminary experimental and theoretical data for ozone are also presented. The difference in behavior of ozone compared to NO₂ and CS₂ under Coulombic regime laser fields is discussed. Thus, we can summarize the task and the scope of this thesis in the following way:

- The dynamics of polyatomic molecules subject to high intensity laser irradiation is studied and discussed.
- At laser intensities between $10^{13} 10^{16}$ W/cm² molecules undergo structural deformations, multiple ionization (via field or multiphoton ionization mechanism), and Coulomb explosion. Depending on the estimated value of Keldysh parameter, ionization mechanism will be either field or multiphoton. Mutiple ionization of molecules leads to Coulomb explosion resulting in fragment ions flying in all directions. Experimental studies of angular distributions of these fragments and analysis of the data will reveal information about the geometry of exploding molecular ions, thus, providing dynamical information about the molecules and molecular ions under high intensity laser fields.
- Target molecules in our studies are triatomics important in the atmosphere, such as CS₂, O₃, and NO₂. In our experiments we observed Coulomb explosion for CS₂ and NO₂ and studied the angular distributions of fragment ions following Coulomb explosion. This helped us retrieve structural information about the exploding particles. We do not observe signs of Coulomb explosion for ozone. Possible explanations of this result are discussed in the text.

2.Experimental

The experiments presented here were carried out with a molecular beam (MB) apparatus (See Fig.4) combined with a time-of-flight (TOF) spectrometer and an intense femtosecond laser source. As shown on Figure 4a, there are two electrodes in the vacuum chamber of the MB apparatus, the extractor and the repeller, to extract the resulting fragment ions after the CE, initially moving towards the detector as well as in the backward direction. Figure 4b shows in more detail how the fragment ions fly after CE, how they are extracted, and the splitting in the mass spectrum caused by the CE. The first peak, observed at earlier arrival time in the mass resolved spectrum, is caused by fragments initially moving towards the detector, whereas the second peak is caused by fragment ions originally moving towards the repeller. Rotating the polarization of the laser pulses we can study the angular distributions of the fragment ions and the structural deformations the molecular ions undergo prior to the CE (5,6).

In the case of CS_2 and NO_2 , the samples were introduced using He as a carrier gas, which entrained some of the vapor pressure of the sample (7). The sample and carrier gas (He, 1700 Torr) expanded through the 1-mm diameter aperture in the pulsed valve. A 2-mm diameter skimmer produced the molecular beam which proceeded to the ionization chamber at $\sim 8 \times 10^{-8}$ Torr with valve closed and $\sim 7 \times 10^{-7}$ Torr when the valve was operated at 30 Hz. He flowed through a metallic tank containing the samples. The

voltages on the extractor and repeller were kept at 1800 and 2500 V, with a distance between them of 1.5 cm.

Ozone was generated by passing ultrapure O₂ through a commercial ozonizer and trapped on silica gel (180 g) at isopropyl alcohol/dry ice slurry temperature (– 84° C). At this temperature, above the boiling point of liquid oxygen, only O₃ is trapped and no further steps are needed to separate it from O₂ (8). Figure 5 shows the container with the ozone trapped on silica gel in a dry ice/isopropyl bath (9). The He carrier gas flowed through the silica gel ozone trap and expanded through the pulsed valve. The skimmer produced the molecular beam, which proceeded to the ionization chamber.

The experiments were performed using a colliding pulse mode-locked dye laser (CPM), pumped by a CW Nd:YLF laser. The output from the CPM was amplified by a four-stage dye amplifier pumped by a 30-Hz Nd-YAG laser, resulting in 60 fs and 200 μJ pulses centered at 620 nm (2 eV/photon). For the CE experiments, the forth dye stage was double-passed to obtain up to 0.5 mJ pulses with a longer duration of ~80 fs. The laser beam was focused on the molecular beam by an f=150 mm lens. The focal spot size of the beam was estimated (Gaussian beam optics) at 20 μm, the measured size (from a burn mark) was 26 μm. Laser pulse intensity was varied from 0.25 to 0.49 mJ, giving a peak power at the focus from 4.6 to 9×10¹⁴ W/cm². The ions formed in the interaction region traveled in a drift free zone (50 cm) before being detected by a micro-channel plate. Twenty time-of-flight mass spectra (TOF-MS) were averaged before analysis. The polarization dependence of the ion intensities was obtained by a zero-order half-wave plate, which was rotated manually from 0 to 180° in 15° increments with respect to the TOF axis. A calcite polarizer was used to ensure high polarization purity of the beam.

3. Experimental Results

A. Experimental results of Coulomb explosion in CS₂ and NO₂. In Figure 6a, we show the TOF-MS resulting from excitation with pulses with 4.6*10¹⁴ W/cm² peak intensity. In addition to the singly and doubly charged molecular ions (CS₂⁺, CS₂²⁺) multiple fragments are observed. We distinguish the singly ionized fragments (C⁺ and S⁺) from the doubly ionized fragments (C²⁺ and S²⁺). In Figure 6b, we show the ionization yield of the CS_2^+ molecular ion as a function of the polarization vector of the excitation beam. Notice that the yield is isotropic, as expected, because of the isotropic distribution of CS₂ molecules in the molecular beam. The data in Figure 6b serve also to confirm that there is no systematic bias in the probability of ion detection as a function of the polarization vector of the excitation field with respect to the time-of-flight axis. A similar isotropic distribution was observed for the CS₂²⁺ ion. The angle - dependent ionization yield for S⁺ and for C⁺ was measured, and the results are presented in Figure 7a in Cartesian and polar coordinates. The experimental data obtained for three separate runs are depicted as circles, squares, and triangles. The lines are best fitted by cosine or sine functions to the fourth power. Notice that the yield for S⁺ follows a cosinusoidal distribution, with maxima at zero and 180° (see Figure 7a). The yield for C⁺ ions follows a sinusoidal distribution with maxima at 90 and 270° (see Figure 7a). The angle dependent ionization vield for S²⁺ and for C²⁺ was measured, and the results are presented in Figure 6b in Cartesian and polar coordinates. The experimental data obtained for three separate runs

are depicted as circles, squares, and triangles. The lines are best fitted by cosine or sine functions to the fourth power. Notice that the yield for S²⁺ follows a cosinusoidal distribution, with maxima at zero and 180°degrees (see Figure 7b). The yield for C²⁺ ions follows a sinusoidal distribution with maxima at 90 and 270° (see Figure 7b). Notice that the results for the doubly ionized fragments show greater sensitivity toward the angle of the polarization vector of the excitation pulse compared to the case of the singly ionized fragments in Figure 7. This indicates the doubly charged particles are ejected from multiply charged molecular ions with more significant bending than that of the singly charged ions. The ionization data shown in Figure 6 are consistent with the angular distribution of the fragment ions obtained with a titanium sapphire laser centered at 800 nm (10). Similarly, we are able to interpret our data in terms of a molecular structure deformation that is consistent with bending.

In Figure 8, we show the mass spectrum of NO_2 undergoing CE. The mass spectrum contains molecular ions, such as NO_2^+ , as well as CE fragments, such as NO^{2+} , N^+ , O^+ , etc. As in our earlier work on CS_2 , performed under similar experimental conditions, some of the peaks are split, which is the signature of CE.

Anisotropic distributions are observed for (a) C^+ and S^+ and (b) C^{2+} and S^{2+} ions in polar and Cartesian plots. Data for three independent experiments (squares, circles, triangles) are accompanied by a guide to the eye (solid line) in the form of a $\cos^4(\theta)$ function. S^+ shows a maximum ion yield at 0° and 180° , while C^+ shows a maximum at 90° and 270° .

B. Preliminary Experimental and Theoretical results for O_3 . An interesting and important molecule to study at high intensity laser fields is ozone (O_3) . The vital role of atmospheric ozone for the biosphere has motivated a large number of experimental and theoretical studies regarding its spectroscopy and electronic structure. However, the behavior of O_3 under the intense laser irradiation has not yet been investigated. Knowledge from such a study would be valuable for predicting the effects high intensity laser pulses might have on the upper atmosphere.

We designed an experiment to study the behavior of ozone under high - intensity laser excitation ($10^{14} - 10^{15}$ W/cm²). As mentioned above, at these intensities molecules undergo multiphoton or field-induced ionization, and the removal of two or more electrons leads to CE. Figure 9a (top) presents the mass spectrum for O₃ taken at a peak power of 4.6×10^{14} W/cm², where ion signals for O₃⁺, O₂⁺, and O⁺ are observed. The data show no evidence of splitting in the fragment ion peaks, which indicates that CE did not occur under these experimental conditions. It should be noted that O₂⁺ and O⁺ signals are partly due to the molecular oxygen present in the molecular beam as a result of ozone decomposition upon the desorption from the silica gel.

Since the absence of CE for ozone was surprising, we increased the laser's peak power up to 9×10^{14} W/cm² (the maximum intensity that could be achieved by the laser system in our experiments), but this increase did not change the spectrum. Our ability to resolve peak splitting depends on the voltage difference between the extractor and repeller. We reduced this difference from 700 V to 200 V. This change did not reveal evidence for fragment ion peak splitting.

The collaboration with Piecuch Group helped us get first and second ionization potentials for O₃ as well as structural data about ozone and its mono- and dications (see Table1).

Table 1. First and second vertical ionization potentials (VIP) of ozone and geometries of O₃⁺ and O₃²⁺ obtained in the CCSD(T) calculations.

O_3^+			
Ionized Electron ^a	Energy (1st VIP)/eV ^b	R(O - O), Å ^c	$\angle O - O - O/degree^{c}$
6a ₁	12.67 (12.85)	1.2371	132.44
4b ₂	12.82 (12.99)	1.2733	104.23
1a ₂	13.39 (13.56)	1.2912	112.81
O ₃ ²⁺			
Ionized Electrons ^a	Energy (2 nd VIP)/eV ^b	R(O - O), Å ^c	∠O – O – O/degree ^c
6a ₁	35.37 (35.62)	1.1749	180.00
4b ₂	35.25 (35.51)	d	d
1a ₂	38.54 (38.75)	1.3437	107.34

^a The three highest occupied orbitals of O₃ are 6a₁, 4b₂, and 1a₂.

^b Calculated with the cc-pVTZ and aug-cc-pVTZ basis sets (the latter results in parantheses). The experimental first and second VIPs are 12.43 eV (S Katsumata, H Shiromaru, T Kimura: Bull. Chem. Soc. Jpn. 57 (1984) 1784) and 34.3 eV, respectively.

^c Calculated with the cc-pVTZ basis set. For comparison, the experimental geometry of ozone is R(O - O) = 1.272 Å, and ∠ (O – O – O) = 116.8 ° (S Katsumata, H Shiromaru, T Kimura: Bull.Chem.Soc.Jpn. 57 (1984) 1784, K Kimura, S Katsumata, Y Achiba, T Yamazaki, A Iwata: Jap. Sci. Soc. Press. (1981)). The optimum geometry could not be determined.

4. Discussion

Let us examine the behavior of triatomics (as an example we take CS₂) in the molecular beam subject to high intensity laser irradiation. If the molecules remained linear, a case depicted in Figure 9a, the signal from the S⁺ ions would show a marked anisotropy. The anisotropy would result from two situations. When the electric field vector is aligned with the TOF axis, the S⁺ ions are ejected toward and away from the detector. Because of the repeller plate, the fragments that are ejected away from the detector are deflected back toward the detector. This leads to a well-known splitting in the ion signal, evident in the zoomed inset of the mass spectrum in Figure 5 for S²⁺ ions. and used in photofragment spectroscopy analysis (11). Note that molecules perpendicular to the field are not affected by the field and yield no ions. When the field is perpendicular to the TOF axis, the S⁺ ions are ejected at a high velocity in a direction that is perpendicular to the TOF axis. Despite the acceleration voltage, the Coulomb repulsion is significant, and in the time it takes those ions to reach the detector plane (estimated to be ~4 us), they are already several centimeters apart and are not detected. For this reason, the S⁺ ions show a distribution that can be simulated by a cosinusoidal function. For linear molecules, the detection of C⁺ ions is not affected by the angle of the polarization vector of the electric field. The predicted detection is therefore isotropic, a fact that is not supported by the data shown in the experimental data in Figure 7. In Figure 10b, we consider the angle dependent detection of fragment ions resulting from bent CS₂ molecules. Unless the bending angle is very large, there is almost no change in the anisotropic dependence of the S⁺ ions discussed above for linear molecules; see Figure 9b, top. However, for bent molecules the C⁺ signal becomes anisotropic. The anisotropy results from the following observations, based on the assumption that the bending angle is small and that the polarizability of the molecule remains along the two S atoms. When the electric field vector is aligned parallel to the TOF axis, the bent CS₂ molecules can have the two S atoms oriented parallel with the field or perpendicular to the field. If the molecules are oriented along the field, then the C⁺ ions are ejected in a direction that is perpendicular to the detector and, thus, will miss it. When the electric field vector is aligned perpendicular to the TOF axis, the bent CS2 molecules oriented along the field eject C⁺ ions toward the detector and register a maximum signal. When the molecules are oriented perpendicular to the field, the signal is minimal because the perpendicular component of the polarizability is very small for small bend angles. From this analysis so far, it is clear that C⁺ ions are predicted to show anisotropic detection that is perpendicular to that observed for S⁺ ions if the CS₂ molecules are bent. The predicted anisotropic ion signal from the Coulomb explosion from bent CS2 molecules is shown in Figure 10. A simple simulation of the parallel and perpendicular components of the polarizability as a function of the bend angle leads us to estimate the bend angles from the singly and doubly ionized data sets to be 170° and 155°, respectively. The agreement between the findings of Iwasaki et al. using mass - resolved momentum imaging (MRMI) and the 800-nm excitation wavelength and our angle determination is good (12).

Similar analysis may be performed for other linear and bent molecules, such as NO₂, SO₂, CO₂, etc. The molecules have isotropic distributions in the molecular beam;

however, there is a clear directionality in the angular distributions (Fig.10), where the maxima of the signals for the fragment ions are reached in the case of parallel or perpendicular polarizations. This result is due to the phenomenon called enhanced ionization (13,14); the ionization is enhanced for the molecules that are aligned in the direction of laser field polarization.

As was mentioned in our Experimental Section, ozone does not undergo CE under the same experimental conditions as NO_2 or CS_2 , a behavior that differs from other similar molecules (such as NO_2 or SO_2). Multiply charged ozone ions are not observed, nor is splitting of the fragment ion signals (See Fig.9). It should be pointed out again that the existence of O^+ and O_2^+ ions in the spectrum may be due to the dissociation of ozone ions as well as to the existence of molecular oxygen in the molecular beam due to the decomposition of O_3 upon the desorption from the silica gel surface. This aspect cannot be addressed quantitatively because of the absence of specific experimental data.

In Figure 8, we showed the mass spectrum of NO₂ undergoing CE. It is interesting that NO₂ and O₃, which have very similar molecular structures, behave differently under the same experimental conditions. What can be concluded from this result is that the response to the high intensity laser field, in the Coulombic regime, is different even for structurally similar molecules. This might be due to the difference in ionization potentials of NO₂ and O₃. However, this is not supported by the experimental and theoretical data available for these molecules (See Table 1 and Table 2). As one can see from Table 2, the experimental values for first and second vertical ionization potentials of NO₂ and O₃ are close (within 1 eV). Therefore, the absence of CE for ozone cannot be due to the ionization potentials.

Table 2. Comparison of experimental values of first and second ionization potentials of O₃, CS₂, CO₂, SO₂, and NO₂.^a

Molecule	1 st ionization potential, eV	2 nd ionization potential, eV
O ₃	12.43	34.3
SO ₂	12.50	34.5
NO ₂	11.23	35.5
CO ₂	13.78	37.7
CS ₂	10.06	27.0

a Ionization potentials taken from F Harris: J. Mass Spec. Ion Proc. 120 (1992) 1, P Millie, I Nenner, P Archirel, P Lablanquie, P Fournier, J Eland: J. Chem. Phys. 84 (1986) 1259, S Katsumata, H Shiromaru, T Kimura: Bull. Chem. Soc. Jpn. 57 (1984) 1784, S Katsumata, H Shiromaru, K Mitani, S Iwata, K Kimura: Chem. Phys. 69 (1982) 423, K Kimura, S Katsumata, Y Achiba, T Yamazaki, A Iwata: Jap. Sci. Soc. Press. (1981), I Griffiths, D Parry, F Harris: Chem. Phys. 238 (1998) 21, P Fournier, J Eland, P Millie, S. Svensson, S Price, J Fournier, G Comtet, B Wannberg, L Karlsson, P Baltzer, A Kaddouri, U Gelius: J. Chem. Phys. 89 (1988) 3553.

One might explain the result by analyzing the stability of the ozone ions, particularly the ozone dication O_3^{2+} , and their dissociation pathways. Generally, but not exclusively, molecular dications are energy-rich species with few long-lived electronic states (15). Usually dication electronic states lie above the thermodynamic asymptote for charge separation so any states possessing a potential barrier to fragmentation are metastable. Figure 10 presents a general schematic illustrating typical potential energy curve for a diatomic dication. One may think of the dication energy curve as being a result of the repulsive Coulombic potential superimposed on the potential curve of the diatomic. Depending on the depth of the minimum in the potential energy curve of the diatomic species, the minimum for the dication curve will be either deep or shallow. Thus, some of the molecules may have metastable dications whereas others may have unstable ones (16).

This implies that stability properties of the dication are determined by the competition between the chemical bond energy and the Coulomb repulsion strength. We assume that the absence of O_3^{2+} in the spectrum and CE may be due to the lifetime of O_3^{2+} . It needs to be less than the acceleration time within the repeller and extractor plates (in ns time scale), but more than the rotational dephasing time (estimated at ~ 5 ps, assuming $T_{rot} = 10$ K). However, this needs further experimental and theoretical studies of ozone subjected to high intensity laser fields in the Coulombic regime.

Another reason for the observed difference in behavior of structurally similar molecules may be due to the laser wavelength dependence of multiphoton ionization. Multiphoton ionization is facilitated for photons with wavelengths that are resonant with excited states of the molecule (See Fig.2). Thus, the wavelength of the laser used might also affect the probability of multiple ionization and Coulomb explosion. For instance, He is doubly ionized at lower peak powers of the laser centered at 780 nm compared to laser centered at around 614 nm (17, 18). Therefore, careful experiments performed at wavelengths in infrared (around 780 nm) would be necessary to address this aspect. In addition, the availability of a laser system such as Ti:Sapphire centered at 780 or 800 nm that would produce intensities beyond 10¹⁵ W/cm² would allow studying CE for ozone because at these intensities production of highly charged ozone ions would be possible. This would lead to CE because of much stronger Coulombic repulsion and thus would allow studying the dynamics of the changes in geometry of ozone at high laser fields.

5. Conclusions

The behavior of triatomics such as CS₂, O₃, and NO₂ subject to high intensity femtosecond laser fields in Coulombic regime was studied. The experiments were performed in the molecular beam coupled with TOF mass spectrometer. TOF mass spectra of CS₂, O₃, and NO₂ following Coulomb explosion were collected along with the angular distributions of molecular and fragment ions. Anisotropic distributions of fragment ions from Coulomb explosion of CS₂ confirmed the prediction about bending of linear triatomics under high intensity laser fields in Coulombic regime. Analysis of anisotropic distributions of singly and doubly charged carbon and sulfur fragment ions allowed retrieving structural information about the molecular ions of CS₂ undergoing Coulomb explosion. This, in fact, provides information about the dynamic behavior of CS₂ irradiated by high intensity femtosecond laser fields.

Two triatomics with similar structures and close first and second ionization potentials, ozone and nitrogen dioxide, were also studied under similar experimental conditions as CS₂. Whereas we observed Coulomb explosion for NO₂, we did not see any signs of it for O₃. The absence of doubly charged ozone ion in the mass spectrum and the absence of splitting of fragment ions imply that there is no Coulomb explosion for ozone at intensities between 10¹⁴ W/cm² and 10¹⁵ W/cm². This may be due to the inability of our laser pulses to doubly ionize O₃. However, this does not seem likely since we are able to multiply ionize NO₂, which has first and second vertical ionization potentials very

close to those of O_3 , as discussed in the text. It should be noted that the wavelength dependence of multiphoton ionization also might play a role. As discussed in the text, for higher excitation wavelengths (for example, 780 nm) multiphoton ionization is facilitated. Careful experimental studies of ozone at these wavelengths would answer the question whether or not ozone would undergo Coulomb explosion at intensities in Coulombic regime.

Another scenario is that doubly charged molecular ions of ozone have a lifetime shorter than the acceleration time within the repeller and extractor plates (in ns time scale), but longer than the rotational dephasing time (~ 5ps). This assumption needs to be supported by further experimental measurements.

APPENDICES

APPENDIX A

Figure 1

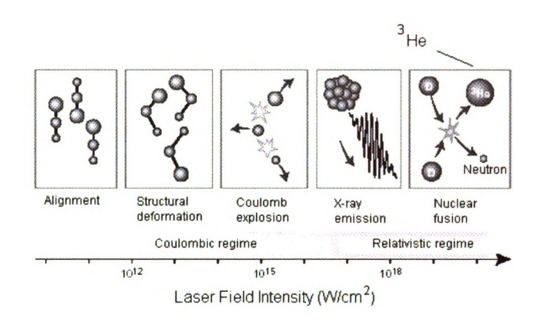


Figure 1. Laser field induced processes in various intensity regimes (from K Yamanouchi: Science 295 (2002) 1659-60).

APPENDIX B

Figure 2

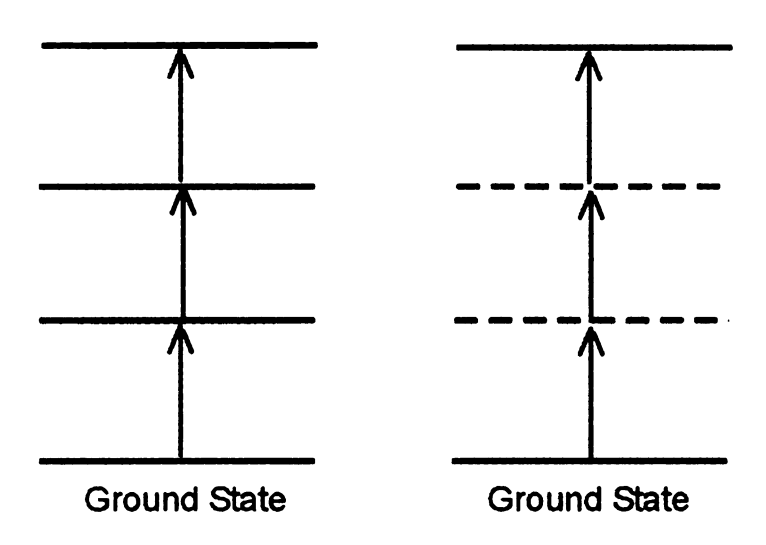


Figure 2. Schematic of 3-step multiphoton ionization in two cases: resonant (on the left) and non-resonant (on the right). Typical laser electric field intensities required for these two processes are $1 - 10^4$ W/cm² and $>10^{12}$ W/cm² for resonant and non-resonant processes respectively. Non-resonant absorption of the photon proceeds through the virtual state with lifetimes on the order of 1 fs.

APPENDIX C

Figure 3

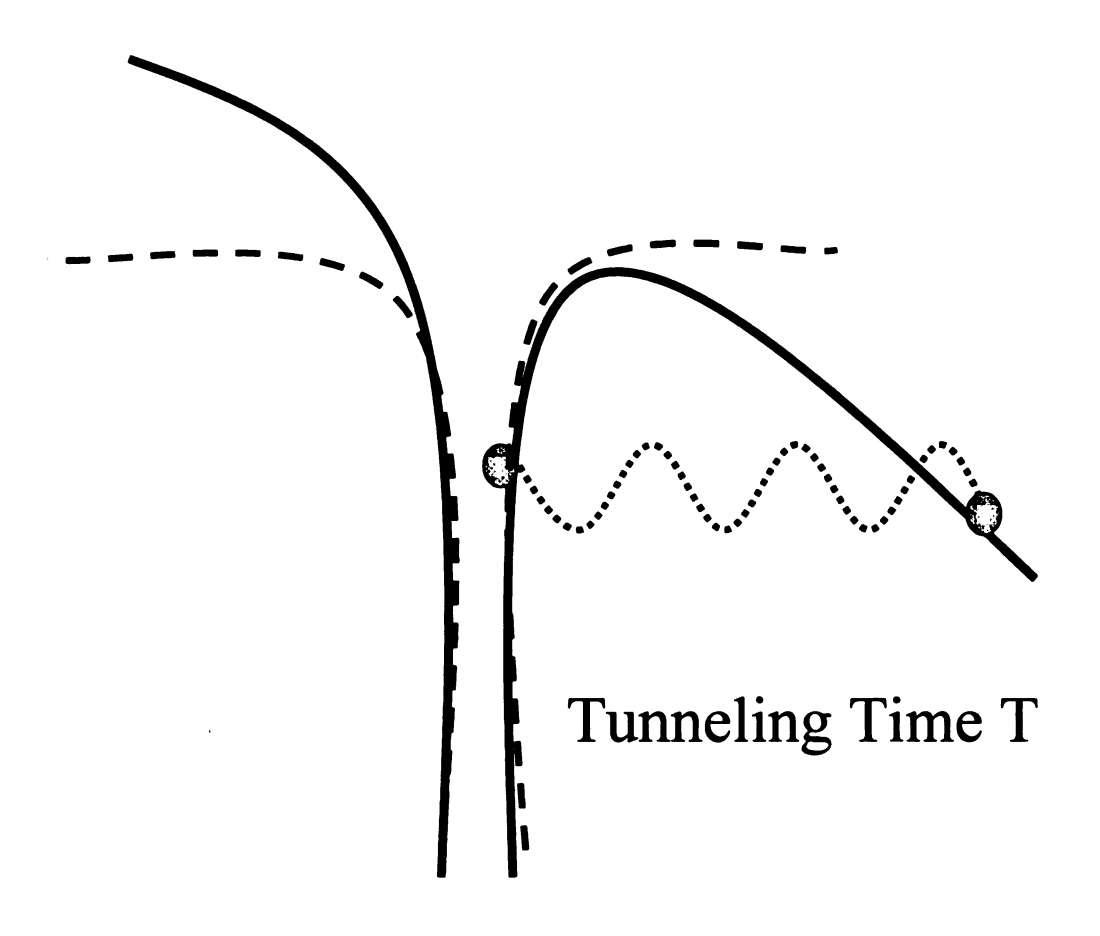


Figure 3. Schematic representation of field (tunneling) ionization for an atomic system. Dashed and solid curves represent the potential energy surfaces in the absence and presence of external electric field respectively.

Keldysh adiabaticity model is reasonable for field ionization when $\gamma = T_{tunnel}/T_{laser} << 1$. In the opposite limit multiphoton ionization mechanism is appropriate.

APPENDIX D

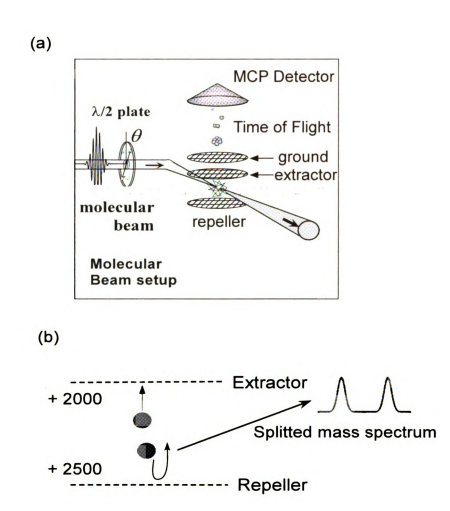


Figure 4. a) Schematic for the experimental setup. b) Schematic representation of the Coulomb explosion process leading to the splitting in the mass spectrum (pointed by the arrow), (from Comstock M, Senekerimyan V, Dantus M: J Phys Chem A 107 (40): 8271 8281 2003).

APPENDIX E

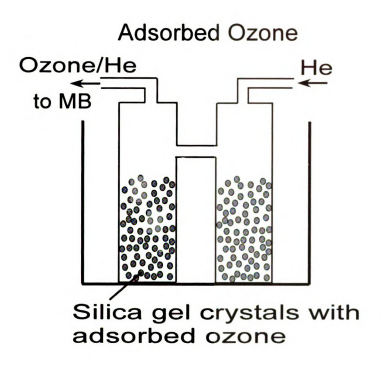


Figure 5. Glass container with the stored ozone on silica gel in the isopropyl/dry ice slurry bath at around - 85° C (from V Senekerimyan, M McGuire, M Comstock, M Dantus: Quantum Control of Light and Matter,. Gordon Research Conference, Mount Holyokee, MA 2003).

APPENDIX F

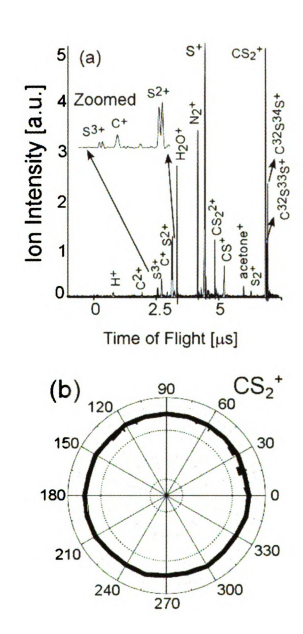


Figure 6. a) Mass spectrum of CS_2 , where the zoomed part shows the splitting of the peaks. b) The isotropic angular distribution of the CS_2^+ parent ion (from Comstock M, Senekerimyan V, Dantus M: J Phys Chem A 107 (40): 8271-8281 2003).

APPENDIX G

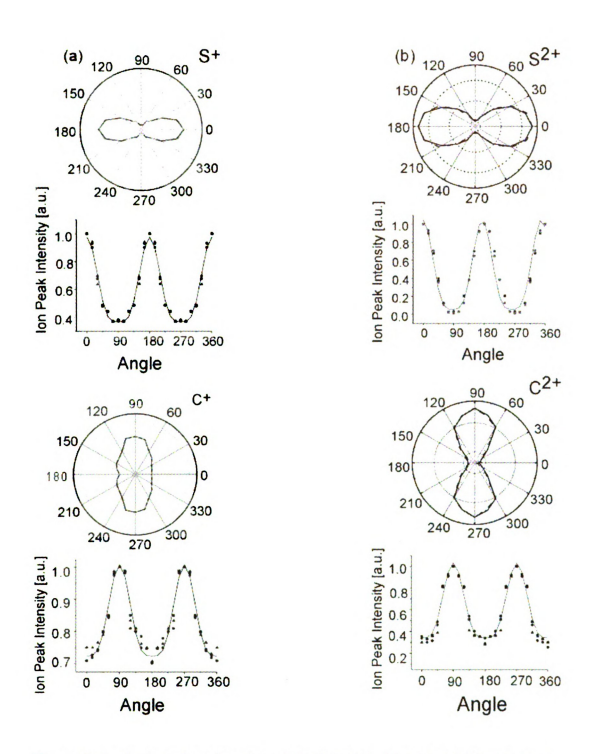


Figure 7. Angle dependent detection of singly and doubly charged fragment ions following Coulomb explosion. pronounced. $.S^{2+}$ shows a maximum ion yield at 0° and 180° , while C^{2+} shows a maximum at 90° and 270° (from Comstock M, Senekerimyan V, Dantus M: J Phys Chem A 107 (40): 8271-8281 2003).

APPENDIX H

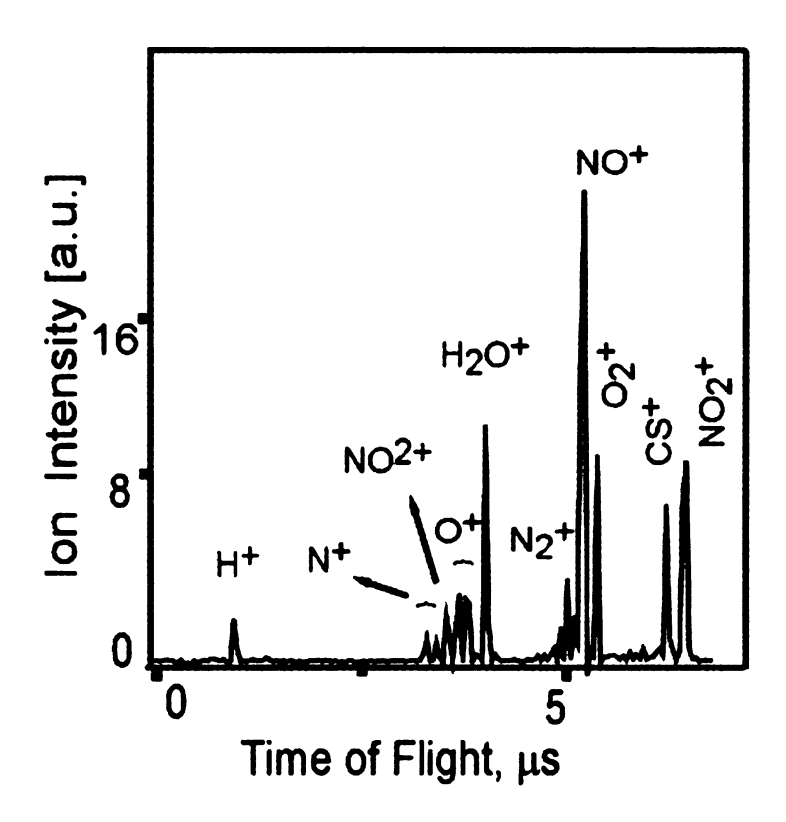


Figure 8. Mass spectrum of NO_2 taken at laser peak power 4.6×10^{14} W/cm². Notice the splitting in the peaks of N⁺ and O⁺ (from V Senekerimyan, M McGuire, MComstock, M Dantus: Quantum Control of Light and Matter,. Gordon Research Conference, Mount Holyokee, MA 2003).

APPENDIX I

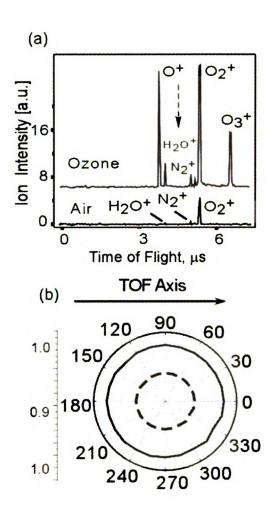


Figure 9. a) Mass spectrum of O_3 (top) and air (bottom) taken under the same experimental conditions as that of NO_2 . The dashed arrow points where $O_3^{2^+}$ should appear. (b) Polar plot of angular distribution for O_2^+ (solid line) and O^+ (dashed line, twice reduced in scale) (from V Senekerimyan, M McGuire, M Comstock, M Dantus: Quantum Control of Light and Matter,. Gordon Research Conference, Mount Holyokee, MA 2003).

APPENDIX J

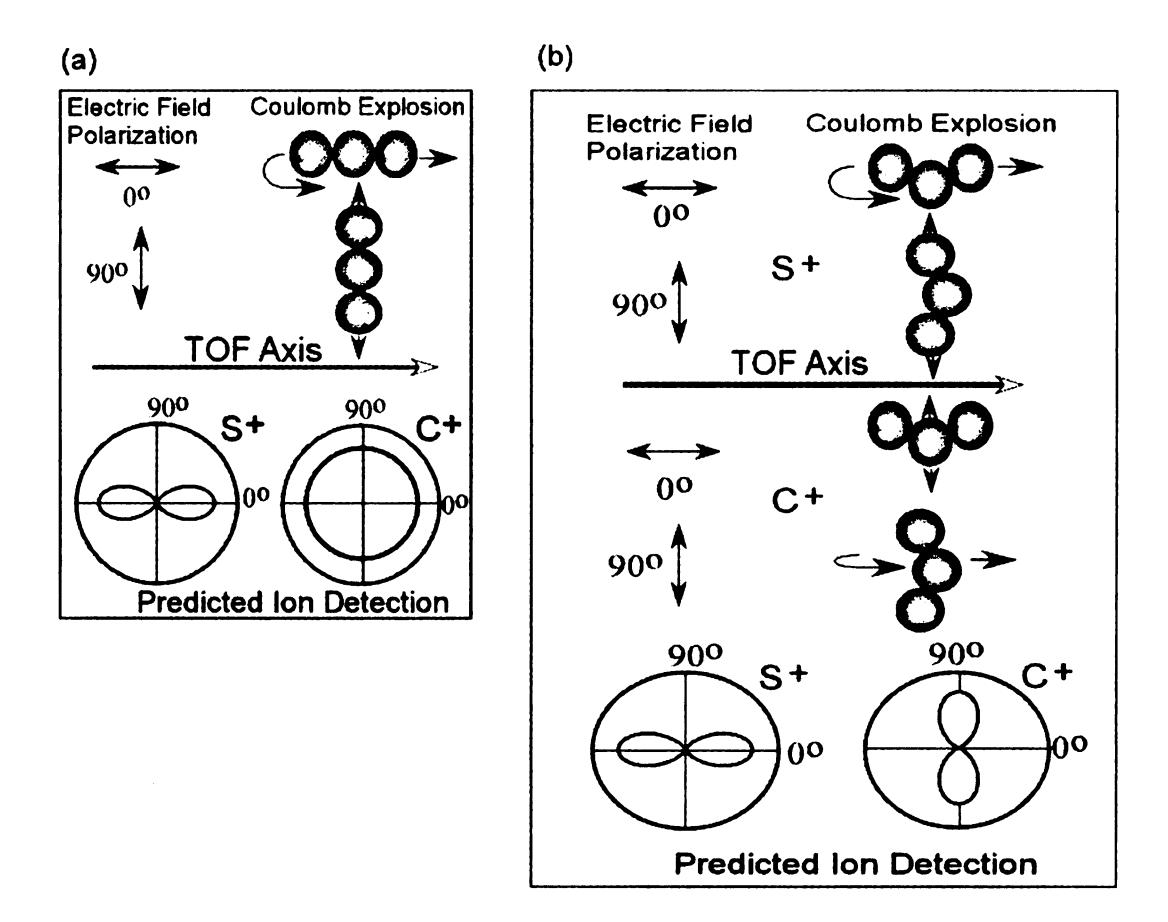


Figure 10. Conceptual drawings of the Coulomb Explosion of CS₂ when the electric field is parallel or perpendicular to the time-of-flight axis for the a) linear molecules and b) bent molecules.

APPENDIX K

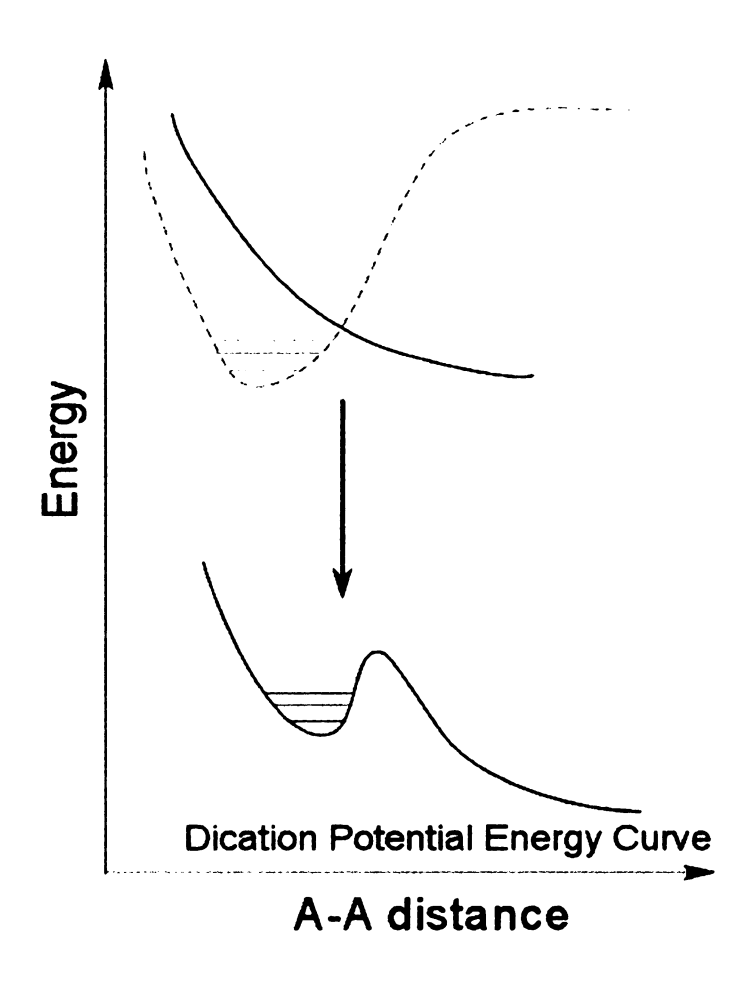


Figure 11. A typical potential energy curve for the diatomic dication.

BIBLIOGRAPHY

- (1) A Zewail: World Scient. series 20th cent. chem. vol. 3. World Scientific.
- (2) L Frasinski, K Codling, P Hatherly: Phys. Lett. A 142 (1989) 499-503.
- (3) Keldysh, Sov. Phys. JETP 20, 1307 (1965).
- (4) K Yamanouchi: Science 295 (2002) 1659-60.
- (5) A Hishikawa, A Iwamae, K Yamanouchi: Phys. Rev. Lett. 83 (1999) 1127-30.
- (6) H Hasegawa, A Hishikawa, K Yamanouchi: Chem. Phys. Lett. 349 (2001) 57-63.
- (7) Comstock M, Senekerimyan V, Dantus M: J Phys. Chem. A 107 (40): 8271-8281 (2003).
- (8) E Coleman, T Siegrist, D Mixon, P Trevor, D Trevor: J. Vac. Sci. Tech. A 9 (1991) 2408-09.
- (9) V Senekerimyan, M McGuire, M Comstock, M Dantus: Quantum Control of Light and Matter,. Gordon Research Conference, Mount Holyokee, MA (2003).
- (10) P Graham, K Ledingham, R Singhal, T McCanny, S Hankin, X Fang, D Smith, C Kosmidis, P Tzallas, A Langley, P Taday: J.Phys.B: At.Mol.Phys. 32 (1999) 5557-74.
- (11) Sander R.K.; Wilson K.R.: J. Chem. Phys. 1975, 63 4242.
- (12) Iwasaki A, Hishikawa A, Yamanouchi K: Chem. Phys. Lett. 2001, 346, 379.
- (13) C Cornaggia, F Salin, CL Blanc: J.Phys. B: At.Mol.Opt.Phys 29 (1996) L749-L54.
- (14) C Cornaggia: Phys. Rev. 54 (1996) R2555-R58.

- (15) P Champkin, N Kaltsoyannis, S Price: J. Electron Spec. and Related Phen. 105 (1999) 21-28.
- (16) D Mathur: Physics Reports 225 (1993) 193-272.
- (17) D. N. Fittinghoff, P.R. Bolton, B. Chang, K. Kulander: Phys. Rev. Lett., 69 18 (1992).
- (18) B. Walker, b. Sheehy, L. Dimauro, P. Agostini, K. Schafer, K. Kulander: Phys. Rev. Lett., 73 9 (1994).

MICHIGAN STATE UNIVERSITY LIBRARIES

3 1293 02732 4841